Supplementary Information

Directional Modified Fluorophores for Super-Resolution Imaging of Target Enzymes: A Case study with Carboxylesterases

Yan Jia[a] §, Jiayue Wang[b], [c]§, Peng Li[d], Xiaochi Ma[b], [c], Keli Han[a]*

[a] Dr. Yan Jia, Prof. Dr. Keli Han. State Key Laboratory of Molecular Reaction Dynamics, Dalian Institute of Chemical Physics, Chinese Academy of Sciences (CAS), Dalian 116023, China. E-mail: klhan@dicp.ac.cn

[b] Dr. Jiayue Wang, Prof. Dr. Xiaochi Ma, Department of Pharmacy, Peking University Shenzhen Hospital, Shenzhen 518036, China.

[c] Dr. Jiayue Wang, Prof. Dr. Xiaochi Ma, College of Pharmacy, Academy of Integrative Medicine, Dalian Medical University, Dalian 116044, China

[d] Prof. Dr.Peng Li, Institute of Molecular Sciences and Engineering, Shandong University, Qingdao 266237, China.

§ These authors contributed equally.

Contents

Part I: Experimental and Theoretical Methods:

Part 2: Schemes, Equations, Tables and Figures

available antibody fluorescent probe targeting specifically hCE1 ($\lambda_{ex} = 488$ nm, images collected from 500-600 nm green channel). Regions of co-localization appeared in cyan (c).

Part 1: Experimental and Theoretical Methods:

1. Synthesis and characterization of the compounds

1.1 General information

1．1．1 Materials

All commercially available reagents, solvents were purchased from Sigma Aldrich, J&K chemicals, Aladdin, Energy Chemical, selleck, cayman and used without further purification. 4-Amino-1,8-naphthalic Anhydride was purchased from Quzhou AMK BioTech Co., Ltd.. Paraoxonase-1 and paraoxonase-2 were obtained from Bioworld (MN,USA). Acetylcholinesterase (AChE, C1682), butyrylcholinesterase (BChE,B4186), alkaline phosphatase (ALP), acid phosphatase (ACP), IgG, transferrin, fibrinogen and α-antitrypsin were all purchased from Sigma-Aldrich (MO,USA) and used as received. The recombinant hCES1 and hCES2 were purchased from Research Institute for Liver Diseases (shanghai) Co.Ltd. Human serum albumin (HSA) was obtained from Solarbio Life Sciences. Rabbit primary Anti-Liver Carboxylesterase 1 (ab45957) was purchased from abcam. Goat anti-Rabbit IgG (H+L) Cross-Adsorbed Secondary Antibody DyLight 488 (Product Invitrogen #35553) and Nucview Red Live were purchased from KeyGEN. All compounds are >95% pure by HPLC analysis.

1.1.2 Instrumentation

Spectroscopic data was measured on the Thermo Scientific™ Varioskan™ Flash Multimode Reader (Thermo, USA). NMR spectra were recorded on a Bruker 400 MHz/500 MHz spectrometer. Both were available at DICP (Dalian Institute of Chemical Physics, Chinese Academy of Sciences) research facilities center. ^{1}H and ^{13}C chemical shifts were reported relative to the residual solvent peak and given in ppm. s: singlet, d: duplet, t: triplet, q: quartet, bs: broad signal, m: multiplet. Confocal fluorescence images were observed with Olympus FV1000 confocal laser-scanning

microscope in our group. Super-resolution images were performed by Nikon N-SIM 5.0 Super-Resolution Microscope System with a motorized inverted microscope ECLIPSE Ti2-E, a 100 × / NA 1.49 oil immersion TIRF objective lens (CFI HP), LU-NV series laser unit (405 nm, 488 nm, 561 nm, 647 nm), and an ORCA-Flash 4.0 SCMOS camera (Hamamatsu Photonics K.K.) in Beijing Institute of zoology, Chinese Academy of Sciences.

1.2 Detailed synthetic procedures of NIC series

1.2.1 Detailed synthetic procedures of NIC-1

Compound 1 0.5g（1.86mmol）was suspended in 20 mL 1,4-Dioxane and 4-Chlorobutyryl chloride 206uL (1.86mmol), EtN3（774uL，5.58mmol）was added. The mixture was refluxed for several hours and the reaction was monitored by TLC. After complete reaction, the mixture was cooled to room temperature and the solvent was evaporated on rotary evaporator until dry. The solid was purified by column chromatography on silica gel using dichloromethane. Yield: (0.50 g, 72% yield). LC-MS (API-ES): m/z $C_{20}H_{21}ClN_2O_3$ [M+H$^+$] 372.13, found 373.13. ^{1}HNMR (400 MHz, CHLOROFORM-D) δ(ppm): δ= 8.62 (d, 1H, J= 7.2 Hz), 8.58 (d, 1H, J= 8.4 Hz), 8.38(d, 1H, J= 8.0 Hz), 8.18 (d, 1H, J= 8.4Hz), 7.93 (s, 1H), 7.77 (t, 1H), 4.17 (t, 2H, J= 5.2 Hz), 3.74 (t, 2H, J= 7.6 Hz), 2.80 (t, 2H, J= 5.6 Hz), 2.30 (m, 2H, J= 5.6 Hz), 1.70 (m, 2H), 1.46 (m, 2H), 0.98 (t, 3H, J= 8.0 Hz).

1.2.2 Detailed synthetic procedures of NIC-2

Compound 2 0.5g（1.86mmol）was suspended in 20 mL 1,4-Dioxane and 2-Chloroethyl chloroformate 232uL (1.86mmol), EtN3（774uL，5.58mmol）was added. The mixture was refluxed for several hours and the reaction was monitored by TLC. After complete reaction, the mixture was cooled to room temperature and the solvent was evaporated on rotary evaporator until dry. The solid was purified by column chromatography on silica gel using dichloromethane. Yield: (0.55 g, 79% yield). LC-MS (API-ES): m/z $C_{19}H_{19}ClN_2O_4$ [M+H$^+$] 375.10, found 375.10. 1HNMR (400 MHz, CHLOROFORM-D) δ(ppm): δ= 8.64 (d, 1H, J= 7.2 Hz), 8.60 (d, 1H, J= 8.4 Hz), 8.34(d, 1H, J= 8.0 Hz), 8.19 (d, 1H, J= 8.4Hz), 7.80 (t, 1H, J=7.6 Hz), 7.49 (s, 1H), 4.55 (t, 2H,

J= 5.2 Hz), 4.18 (t, 2H, J= 7.6 Hz), 3.81(t, 2H, J= 5.6 Hz), 1.72 (m, 2H), 1.46 (m, 2H), 0.98 (t, 3H, J= 8.0 Hz).

1.2.3 Detailed synthetic procedures of NIC-3

NIC-2 0.1g（0.26mmol）was suspended in 5 mL methol and Tetramethylguanidine 65 uL was added and mixed for 30 min. The reaction was monitored by TLC. After complete reaction, solution was evaporated to dry and the solid was purified by column chromatography on silica gel using dichloromethane. Yield: (0.09 g, 95% yield). LC-MS (API-ES): m/z $C_{19}H_{18}N_2O_4$ [M+H$^+$] 339.13, found 339.13. 1HNMR (400 MHz, Chloroform-d) δ(ppm): δ= 8.64 (d, 1H, J=7.2 Hz), 8.61 (d, 1H, J= 8.0 Hz), 8.28(d, 1H, J= 8.6 Hz), 7.80 (t, 1H, J= 7.8Hz), 7.69 (d, 1H, J=7.6 Hz), 4.71 (t, 2H, J=8.2 Hz), 4.20 (m, 4H), 1.72 (m, 2H), 1.45 (m, 2H), 0.98 (t, 3H, J=7.2 Hz). 13CNMR (100 MHz, Chloroform-d) δ(ppm): 163.90, 163.44, 156.59, 140.13, 131.11, 129.32, 127.78, 127.36, 123.35, 123.29, 122.22, 62.77, 48.68, 40.34, 30.18, 20.37, 13.85.

1.2.4 Detailed synthetic procedures of NIC-4

Compound 3 0.524g（1.86mmol）was suspended in 20 mL 1,4-Dioxane and 4-Chlorobutyryl chloride 206uL (1.86mmol), EtN_3（774uL，5.58mmol）was added. The mixture was refluxed for several hours and the reaction was monitored by TLC. After complete reaction, the mixture was cooled to room temperature and the solvent was evaporated on rotary evaporator until dry. The solid was purified by column chromatography on silica gel using dichloromethane. Yield: (0.469 g, 65% yield). LC-MS (API-ES): m/z $C_{20}H_{21}ClN_2O_3$ [M+H$^+$] 389.12, found 389.12. ^{1}HNMR (400 MHz, CHLOROFORM-D) δ(ppm): δ= 8.63 (m, 2H, J= 7.2 Hz), 8.18 (d, 1H, J= 8.4 Hz), 7.80(d, 1H, J= 8.0 Hz), 7.63 (d, 1H, J= 8.4Hz), 4.43 (t, 2H), 4.17 (t, 2H), 3.94 (t, 2H, J= 5.2 Hz), 3.52 (s, 3H), 2.80 (t, 2H, J= 5.6 Hz), 1.72 (m, 2H), 1.46 (m, 2H), 0.98 (t, 3H, J= 8.0 Hz).

2. Spectroscopic Measurements.

Spectroscopic data was measured either on a Lambda 35 UV-visible Spectrophotometer (Perkin-Elmer), or on a Fluoromax-4 Spectrofluorometer (Horiba-Jobin Yvon), with a Xenon lamp or on the Thermo Scientific™ Varioskan™ Flash

Multimode Reader (Thermo, USA). Data analysis was performed using GraphPrism 5.0. NMR spectra were recorded on a Bruker 400 MHz spectrometer. Both were available at DICP (Dalian Institute of Chemical Physics) research facilities center. ^{1}H and ^{13}C chemical shifts are reported relative to the residual solvent peak and are given in ppm. s: singlet, d: duplet, t: triplet, q: quartet, bs: broad signal, m: multiplet. Confocal fluorescence images were observed with Olympus FV1000 confocal laser-scanning microscope.

3. Enzyme kinetic assay

The reaction was initiated by adding NICs in 100% DMSO (2 μl) to preincubated hCEs (198μl, 0.1mg/mL, phosphate buffer solution, PH=7.4), at a final concentration of 0.1 to 50 μM. The reaction between NIC and hCEs took place at 37°C. Incubation proceeded for 10 min and the emission intensity at 530 nm was immediately detected using Thermo Scientific™ Varioskan™ Flash Multimode Reader (Thermo, USA).

Michaelis-Menten equation analysis is applied.

$$v = \frac{v_{max} \times [S]}{k_M + [S]}$$

Here, $[S]$ is the concentration of substrate. K_M is the apparent enzyme kinetics parameters michaelis constant, v_{max} is the maximum velocity.

The linear relationship between $\frac{1}{v}$ and $\frac{1}{S}$ named as Lineweaver-Burk plot is also applied.

$$\frac{1}{v} = \frac{1}{v_{max}} + \frac{k_M}{v_{max} \times [S]}$$

4.Enzyme Selectivity Study

Stock solutions of 50mg/mL HSA, 1mg/mL hCE1/hCE2/PON1/PON2, AChE 200μg/L, BChE 400U/L, 50 mg/mL pepsin/trypsin/chymotrypsin, 50 mg/ml transferrin/lg G/fibrinogen/ A1AT, 2 μM ALP/ACP were prepared in distilled water and stored in frozen aliquots at -20℃. Slow thaw on ice, diluted to specified concentration just before experiment and each one could only be thawed once. Stock

solution of NIC-1/2/3/4 were prepared in DMSO and diluted in phosphate buffer solution (pH=7.4) to specified concentration when used. Enzyme solution (10 μL) was mixed with the substrate (2μL) solution in PBS buffer (pH 7.4, 188μL). Fluorescence intensity at 520nm was recorded after incubation for 2h at 37℃ using the fluorescence plate reader.

5. Enzyme Inhibition Study

Inhibition experiments were performed in a total volume of 200 μL PBS containing 0.1mg/mL hCEs, 10 μM NIC-1/200 μM 4-NPA, and various inhibitors (from 0.1 μM to 100 μM). Fluorescence emission (Absorbance) from protein-free samples containing substrate and potential inhibitors were subtracted as background. A decrease in fluorescence (Absorbance), indicating inhibition of enzyme activity, was measured after 10 min of incubation with excitation at 450 nm and emission at 520 nm (absorbance at 405nm) on a Thermo Scientific™ Varioskan™ Flash Multimode Reader (Thermo, USA).

IC_{50} values were obtained by fitting data to the below equation, where Y represents the fluorescence (absorbance) signal observed after background subtraction.

$$Y = \frac{100}{1 + 10^{(X - logIC_{50})}}$$

For noncompetitive inhibition type reaction, k_i values were calculated resolving to the non-linear noncompetitive inhibition equation:

$$v_{max}^{Inh} = \frac{v_{max}}{1 + k_i}$$

$$Y = \frac{v_{max}^{Inh} \times X}{k_m + X}$$

v_{max} and k_m represent the maximum enzyme velocity and the Michaelis-Menten constant without inhibitor, whereas v_{max}^{Inh} represents the maximum enzyme velocity for one concentration of inhibitor, and k_i is the inhibition constant.

For competitive inhibition type reaction, k_i values were calculated resolving to the non-linear competitive inhibition equation:

$$k_m^{Obs} = \frac{k_m}{1 + \frac{[I]}{k_i}}$$

$$Y = \frac{v_{max}^{Inh} \times X}{k_m^{Obs} + X}$$

k_m represent the Michaelis-Menten constant without inhibitor, whereas k_m^{Obs} represents the Michaelis-Menten constant in the presence of inhibitor, and k_i is the inhibition constant.

6. Cell culture

Human Hepatocellular Cancer Cell Line Bel-7402 (HL7402) were cultured in RPMI-1640 containing $NaHCO_3$ 1.5g/L, glucose 2.5g/L, Sodium Pyruvate 0.11g/L and 10% FBS. Cells were seeding at a density of 1 × 105 cells per dish (*Φ* 20 mm) and incubated in a humidified incubator containing 5% CO_2 at 37 °C.

7. Cell viability test

HL7402 cells were seeded in each well of 96-well plates at a density of 6.5×10^3 cells/well/100 μL and incubated for 24 h for cell attachment. The stock solution of probe NIC-2/4 was diluted with a cell culture medium containing 10% FBS to have a final concentration of 25/10/5/1/0.1/0.01 μM, respectively. HL7402 cells were treated with probe containing media for 48h. After washing the cells twice, cell viability was measured using SRB assay. After incubation period, cell monolayers were fixed with 10%(wt/vol) trichloroacetic acid and stained for 30 min, after which the excess dye was removed by washing repeatedly with 1% acetic acid. The protein-bound dye was dissolved in 10mM Tris base solution for OD determination at 510nm using a microplate reader (Varioskan Flash, thermo scientific, USA). Cell viability was calculated as a percentage compared to media-treated control cells. Data are expressed as a mean ± standard deviation. For a 48h assay, no significant toxicity was observed.

8. **Confocal Fluorescence Imaging condition.** Confocal fluorescence images were

observed with Olympus FV1000 confocal laser-scanning microscope with an objective lens (×100). For the blue channel, excitation wavelength was set at 405 nm, and blue emission was collected with a 425−475 nm window. For the green channel, excitation wavelength was set at 488 nm, and green emission was collected with a 500-600 nm window. For the red channel, excitation wavelength was set at 635 nm, and green emission was collected with a 647-755 nm window.

9. **SIM imaging.** LU-NV series laser unit (405 nm, 488 nm) are used. Long term SIM imaging were performed by continuous imaging of dozens of minutes at twenty second intervals after 30 min incubation of NIC-4 with HL7402 cells, or cells processing with immunofluorescent staining procedure. Time-lapse images and time-colored images are provided to depict the dynamic movement of targeted movement.

10. **Immunofluorescence Staining and NIC Co-Staining in Fixed Cells.** Immunofluorescence analysis of hCE1 was performed using HL7402 cells. The cells in 35 mm × 12 mm glass bottom cell culture dishes were set at a density of 2.5×10^5 /mL. The cells were fixed with 100% methanol (chilled at -20°C) at room temperature for 5 min, permeabilized with 0.1% Triton™ X-100 for 10 minutes, blocked with 1% BSA for 1 hour and labeled with 2 μg/mL Rabbit primary antibody for 3 hours at room temperature. NIC-4 and NIC-2 was used at the concentration of 5 μM in PBS at room temperature for hCE1 staining test (blue channel imaging). In another group, Goat anti-Rabbit IgG (H+L) Cross-Adsorbed Secondary Antibody DyLight® 488 conjugate was used at a concentration of 2 μg/mL in PBS containing 0.2% BSA for 45 minutes for the labelling of hCE1 in the cytoplasm (green channel imaging). Nuclei were stained with Nucview Red Live (red channel imaging).

11. Living cell imaging

HL-7402 cells imaging has been performed labeled with NIC-2/4. The cells in 35

mm × 12 mm glass bottom cell culture dishes were set at a density of 2.5× 10^5 /mL. After washing the cells with PBS for 3 times, the stock solution of NIC-2/4 in DMSO (1 mM) was diluted with phosphate buffered saline solution (100 mM, pH 7.4, 138 mM NaCl) to the final concentration of 5 μM. The cells were incubated for 0.5h under 37 °C before imaging study. Imaging was collected through the same condition described in the ***Immunofluorescence Staining and NIC Co-Staining in Fixed Cells*** part.

12. Computational Details for the mechanism study

The initial ternary structure of human carboxylesterase-1 (hCE1) was obtained from the PDB database with entry code 2H7C(*1*). Chain A representing monomer was used for simulation. Structure information without ligand was used as receptor for Molecular Docking and Apo-system for blank control. The protonation states of titratable residues were carefully assigned according to the calculated pKa values by PDB2PQR online server(*2*). For histidine involved protonation definition, His468 in the catalytic center was protonated at the δ position. Afterwards, hydrogen atoms were added and optimized using the casual force field ff14SB(*3*) in Amber16 package(*4*). Geometrical optimization for studied ligands 4-NPA and NIC-4 was carried out at level of B3LYP theory(*5*-*7*) with 6-311+G(2d,p)(*8*) basis set in Gaussian 16 A03(*9*). Parameters of the bonds, angles, dihedrals, and van der Waals of the ligand were then fitted based on RESP charges in the force field of generalized Amber force field (GAFF) embedded in Amber16 package. The Auto-Dock Vina program(*10*) and the default parameters were used to obtain series of conformation with 4-NPA and NIC-4 binding to hCE1. The docking box was centered by the Ser221-Glu354-His468 catalytic triad and set to embrace the whole cavity. From the initial docking performance, nine binding models for each ligand were generated and used as the starting conformation set Molecular Dynamics (MD) simulation. The binding models of 4-NPA_hCE1 and NIC-4_hCE1 were fully solvated in the truncated-orthorhombic-shaped boxes. The solvation thickness is at least 10 Å and TIP3P model(*11*) was applied to describe the water molecules. Sodium ions were added to ensure the neutrality. The solvated complexes were relaxed with minimization run to release bad contacts and heated with 200

picoseconds (ps) procedure to reach 300 K. Before the production run, another 200 ps simulation aiming at stretching hydrogen and side chains of the system was executed. The production stage of MD process ran under isothermal−isobaric ensemble condition from which the last 1ns trajectory was used for binding energy calculation. Binding system with the lowest calculated energy value was selected as the representing model for 4-NPA/NIC-4_hCE1. The elongated 20 ns simulation for each of the selected ligand binding model based on which the ligand-protein interaction analysis would carry out was performed. The final 20ns trajectories were used for ligand-protein interaction analysis. Frames with suitable attacking distances for both nucleophilic attack and proton transfer within catalytic center were also selected from the modelled trajectory and used for steered MD (sMD) study. In sMD simulation, the catalytic center including side chains of key residues surrounded by the binding ligand NIC-4/4-NPA (Leu97, Gly142, Gly143, Val146, Ser221, Leu304, Ile359, Leu363, Met364, Phe426, His468 for NIC-4_hCE1 system, Ala93, Leu97, Gly142, Gly143, Val146, Ser221, Leu255, Leu304, Ile359, Met364, Phe426, His468 for 4-NPA_hCE1 system) and complete structure of NIC-4/4-NPA was described with the semi-empirical QM mechanics as self-consistent charge density functional tight binding method (SCC-DFTB)(*12*). The remaining part of each system was treated by the Amber ff14SB force field. The reaction coordinate was set as the distance from nucleophile oxygen O_{Ser221} from hydroxyl group of Ser221 to the carbonyl carbon C_{Ligand} in carboxyl group of 4-NPA and amide group of NIC-4, representing the nucleophilic attack process from Ser221. The reaction coordinate was varied from ~ 2.7 Å to 1.4 Å with force constant set to be 200.0 kcal/mol/Å^2 in 100 ps run. Sampling for the reaction coordinate was dumped every 0.1 ps. The MD simulations were executed under periodic boundary conditions (PBC) with a 2fs time step. Van der Waals and short-range electrostatic interactions were estimated within a 10 Å cutoff. The long-range electrostatic interactions were assessed with the particle mesh Ewald method(*13*). The SHAKE algorithm(*14*) was applied to all bonds including hydrogen atoms.

Part II: Schemes, Equations, Tables and Figures

Table S1. Known substrates and inhibitors of CE with carbamate configuration.

Compound Name	Molecular Structure	CE-1 Substrate	CE-2 Substrate	CE-1 Inhibition	CE-2 Inhibition	Categorization
lidocaine	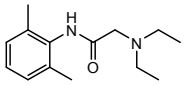	√	-	-	-	R_1-NH-CO-R_2
Irinotecan	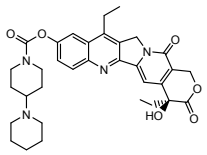	-	√	-	-	R_1-NH-CO-R_2
NCEN	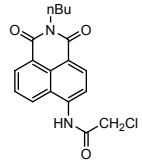	-	√	-	-	R_1-NH-CO-R_2
Flutamide	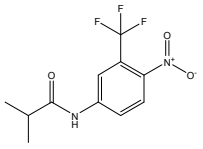	-	√	-	-	R_1-NH-CO-R_2
Eserine(*15*)	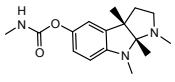	-	-	**1198 μ M**	**0.358 μ M**	R_1-NR_2-CO-R_3

Loperamide (*16*)	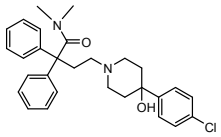	-	-	**440**	**1.5**	R_1-NR_2-CO-R_3
JZL184(*17*)	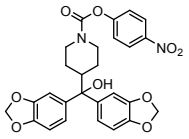	-	-	**0.48 μ M**	**0.63 μ M**	R_1-NR_2-CO-R_3
Phenethylcymserine	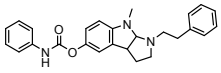	-	-	**20.5 μ M**	**5.6 μ M**	R_1-NR_2-CO-R_3

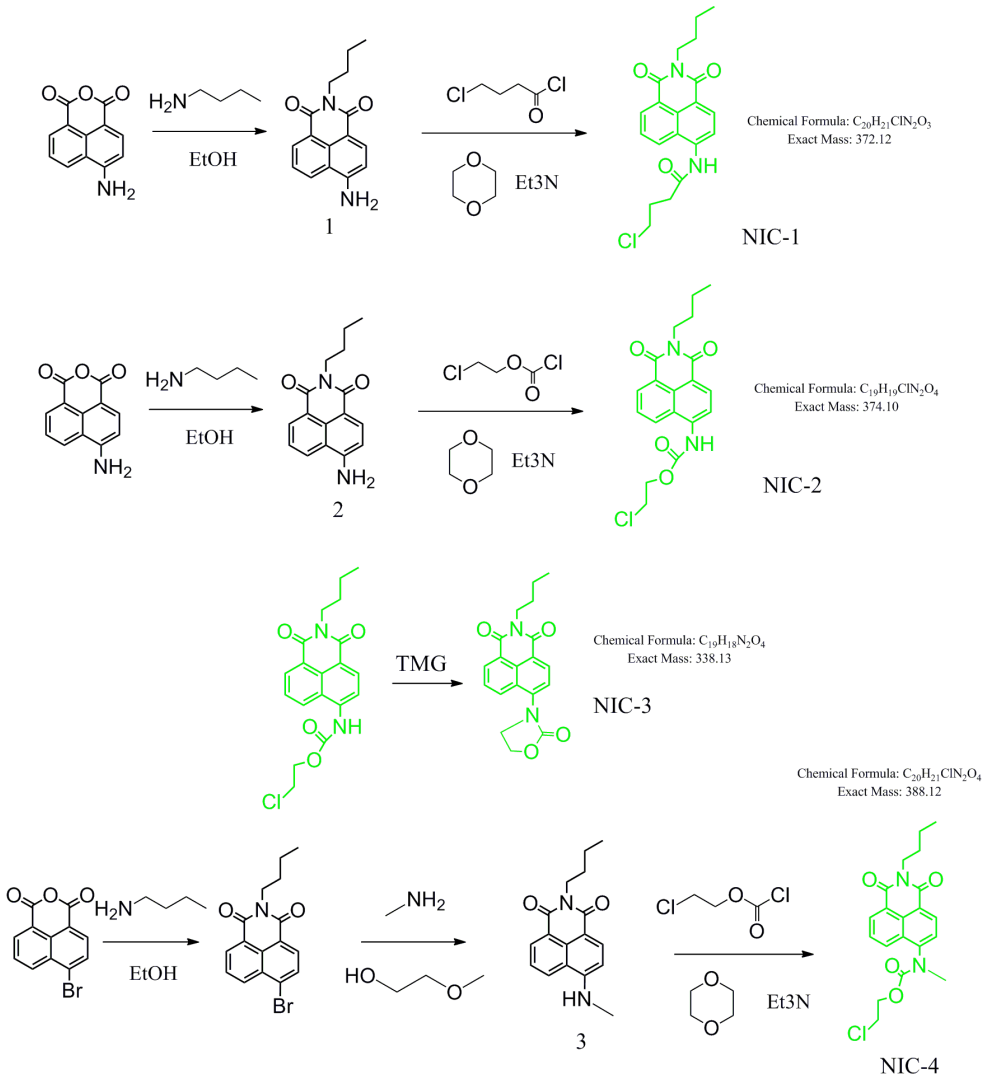

Figure S1. Synthesis process of NIC-1/2/3/4.

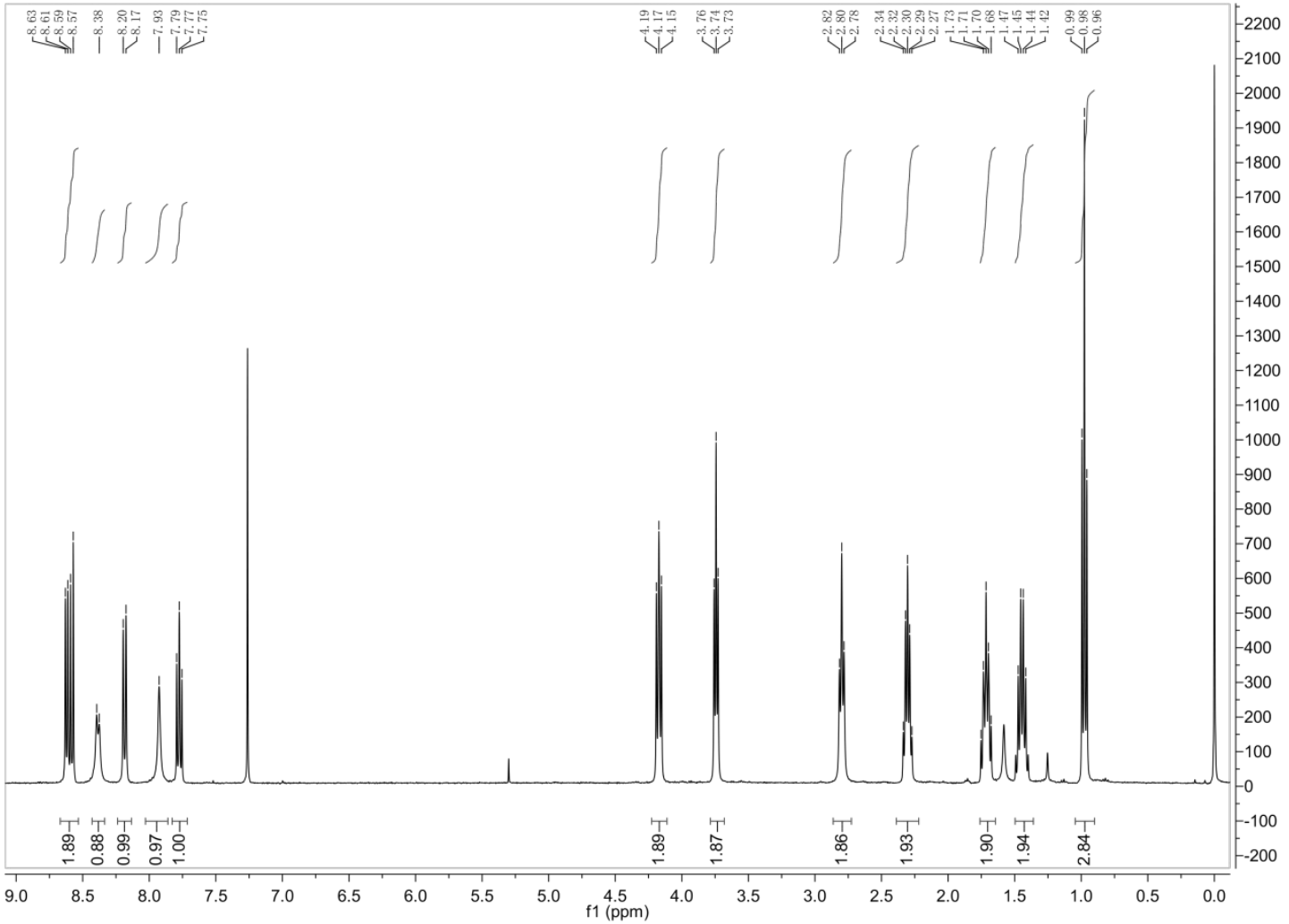

Figure S2. NIC-1 ^{1}H NMR

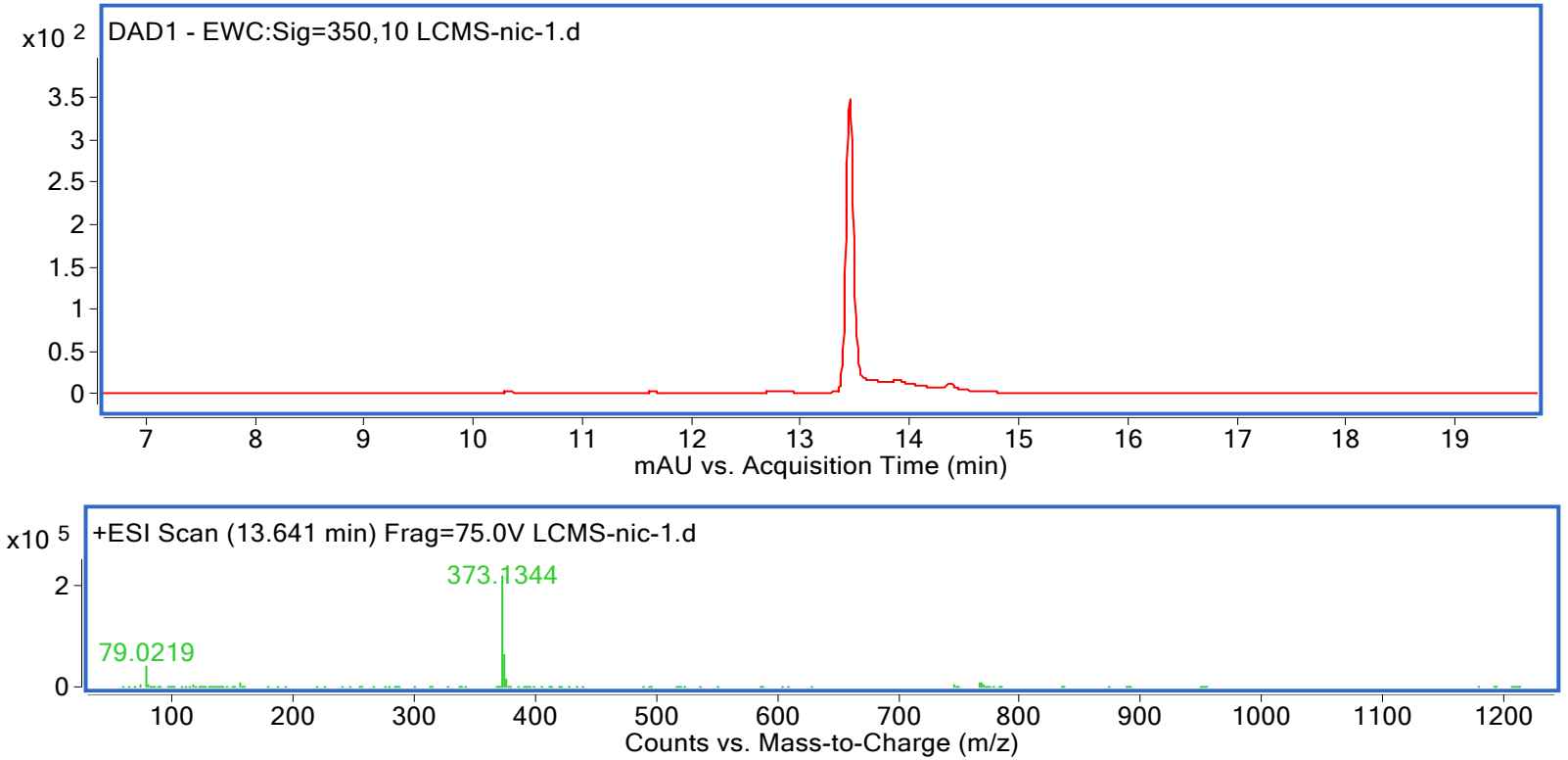

Figure S3. HPLC and HRMS of NIC-1

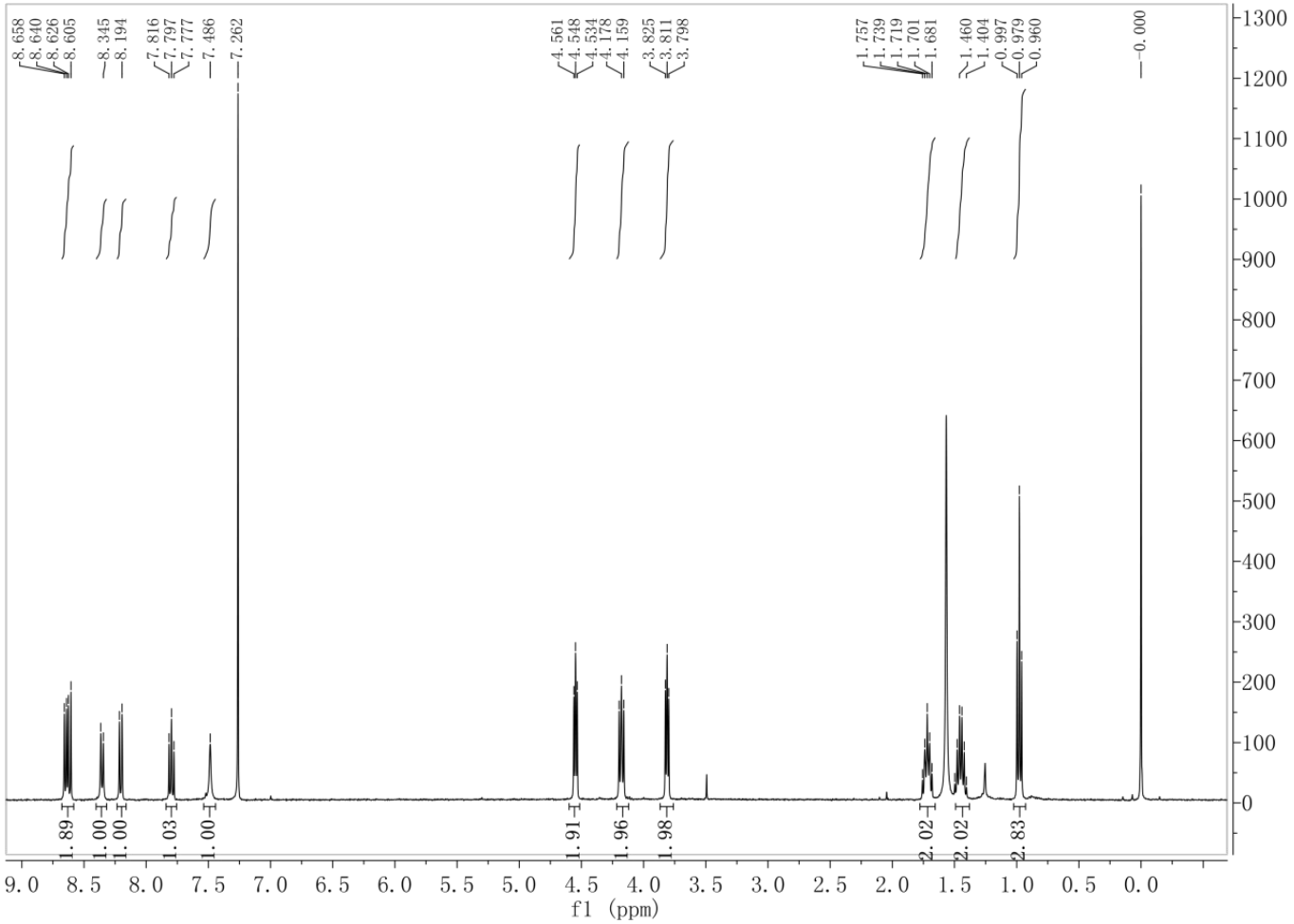

Figure S4. NIC-2 ^{1}H NMR

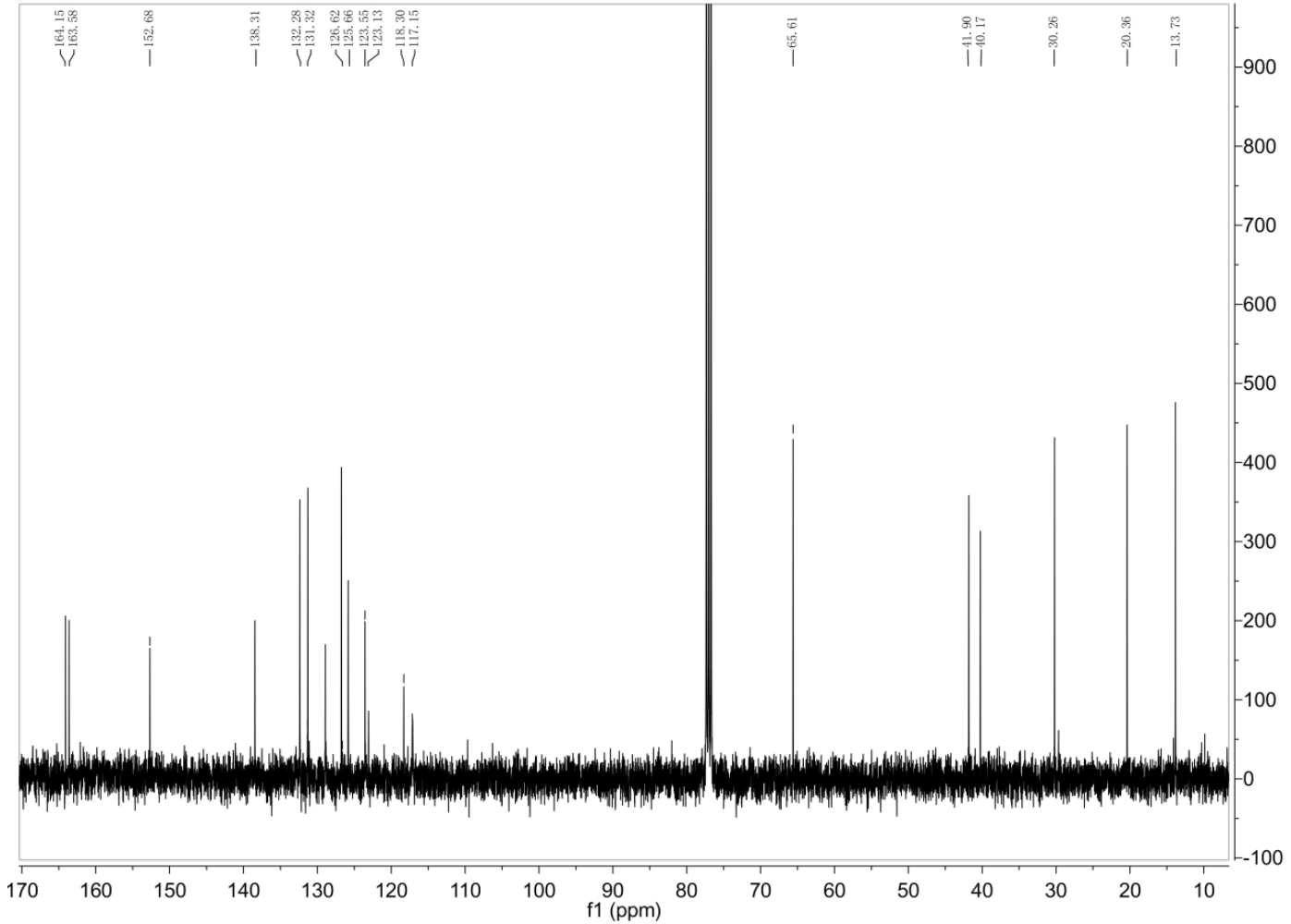

Figure S5. NIC-2 ^{13}C NMR

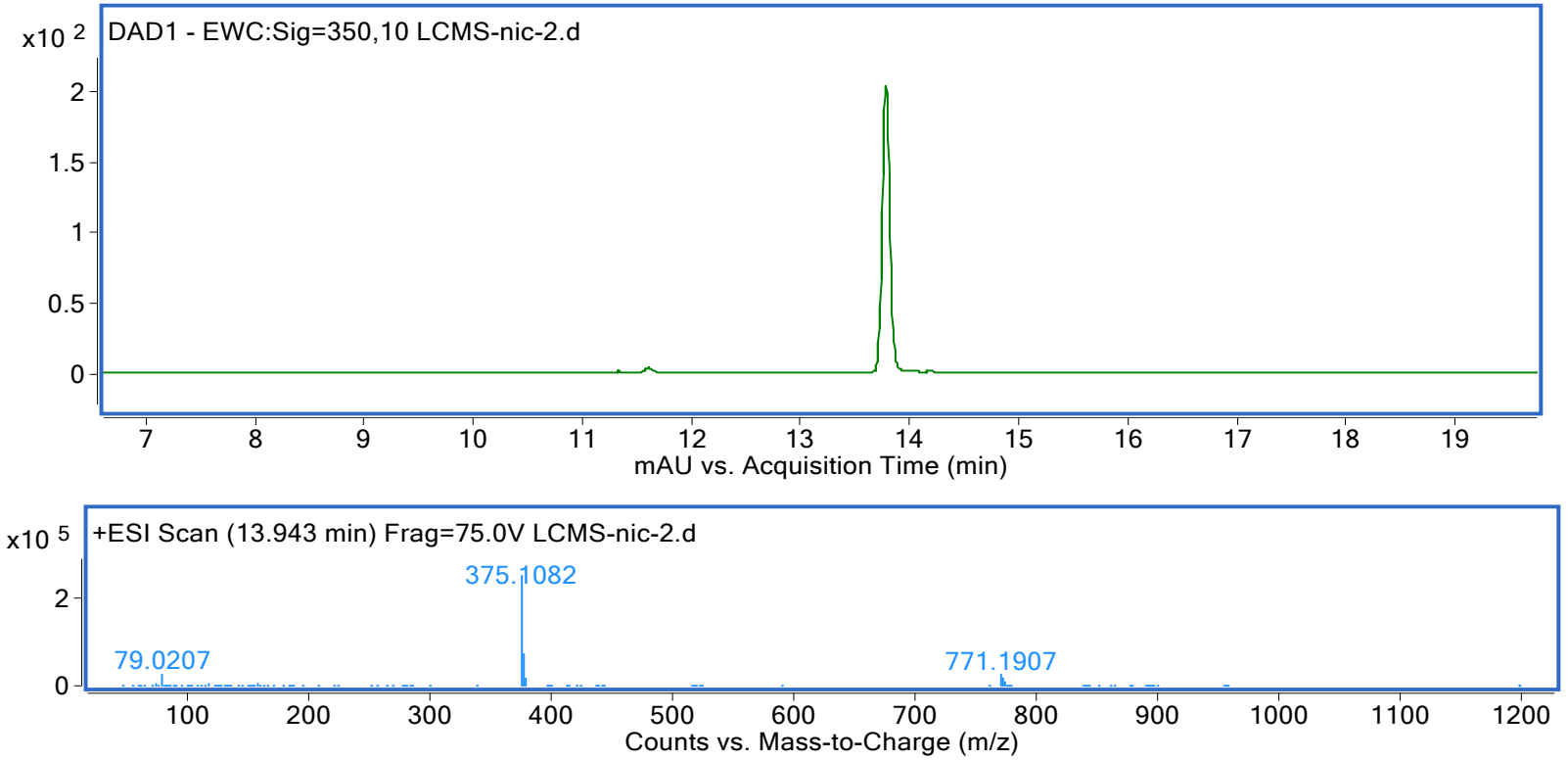

Figure S6. HPLC and HRMS of NIC-2

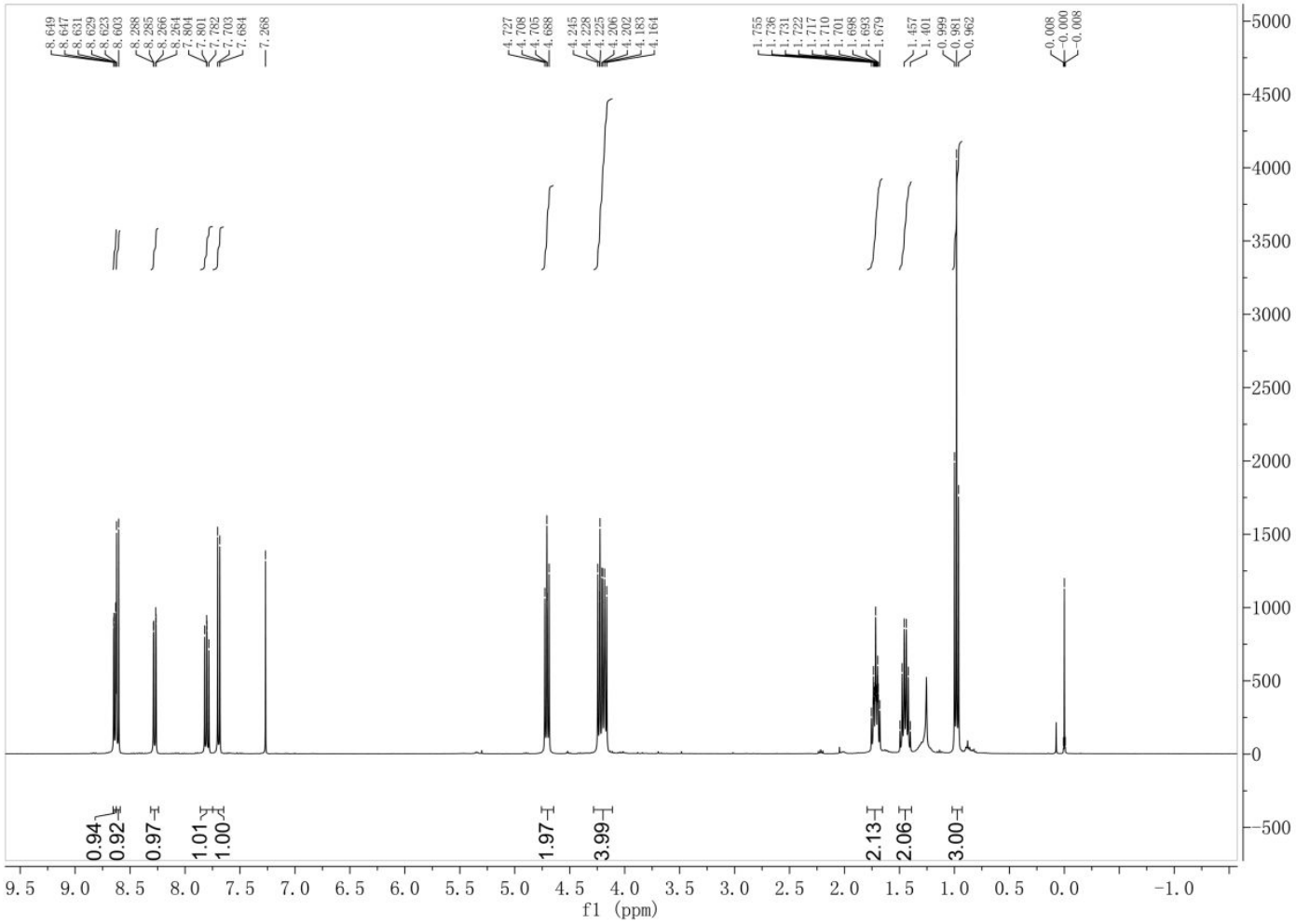

Figure S7. NIC-3 ^{1}H NMR

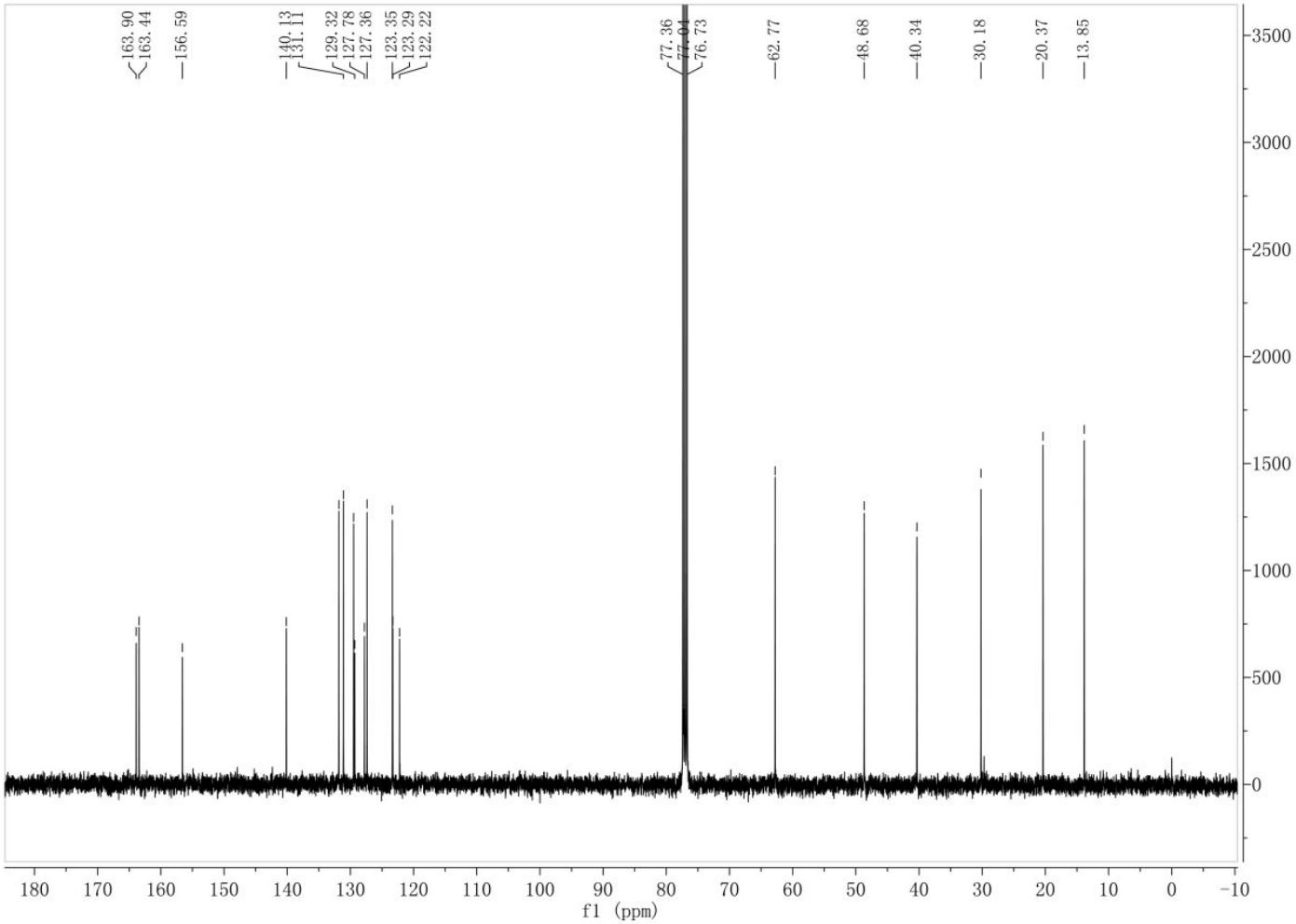

Figure S8. NIC-3 ^{13}C NMR

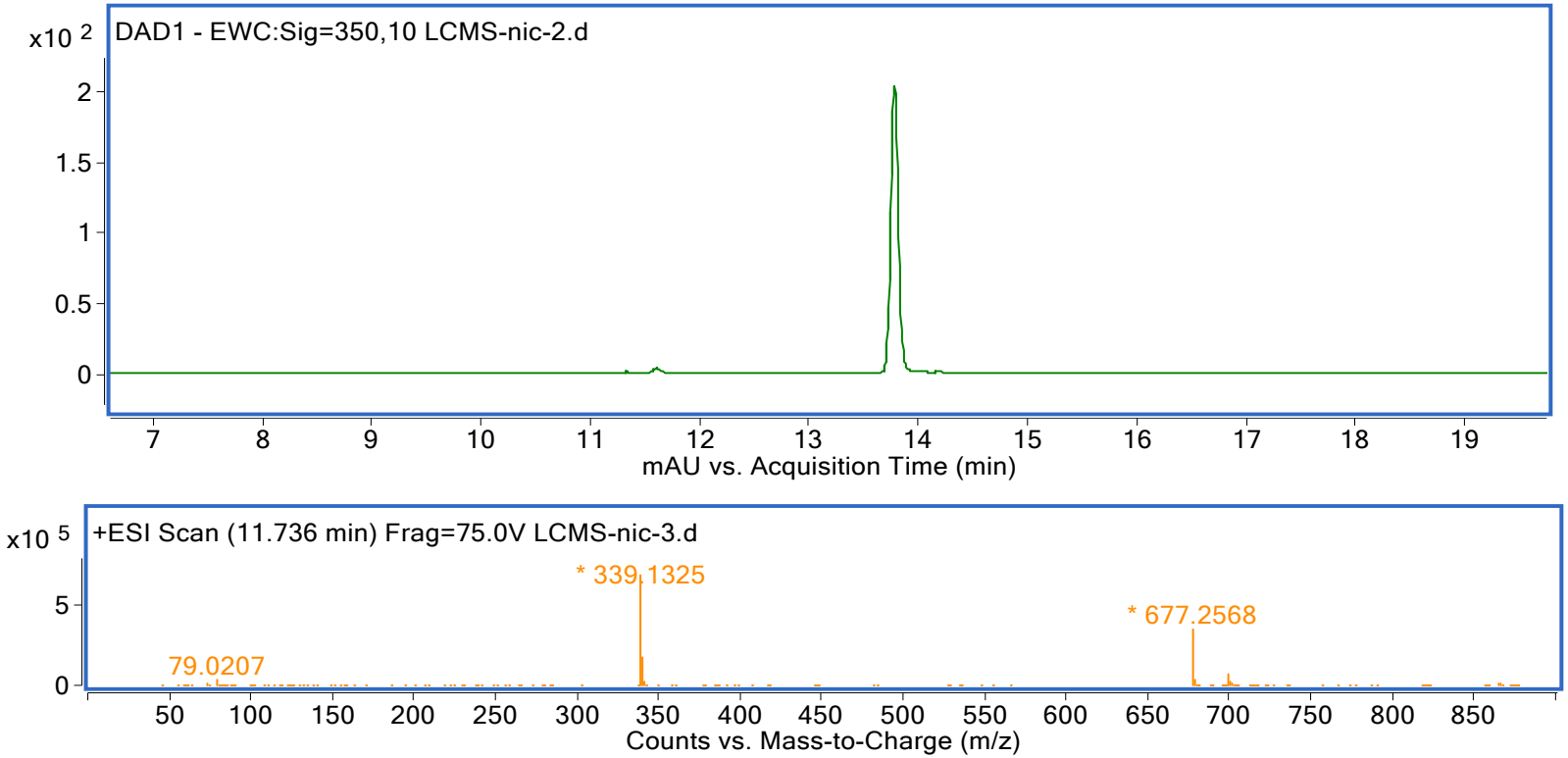

Figure S9. HPLC and HRMS of NIC-3

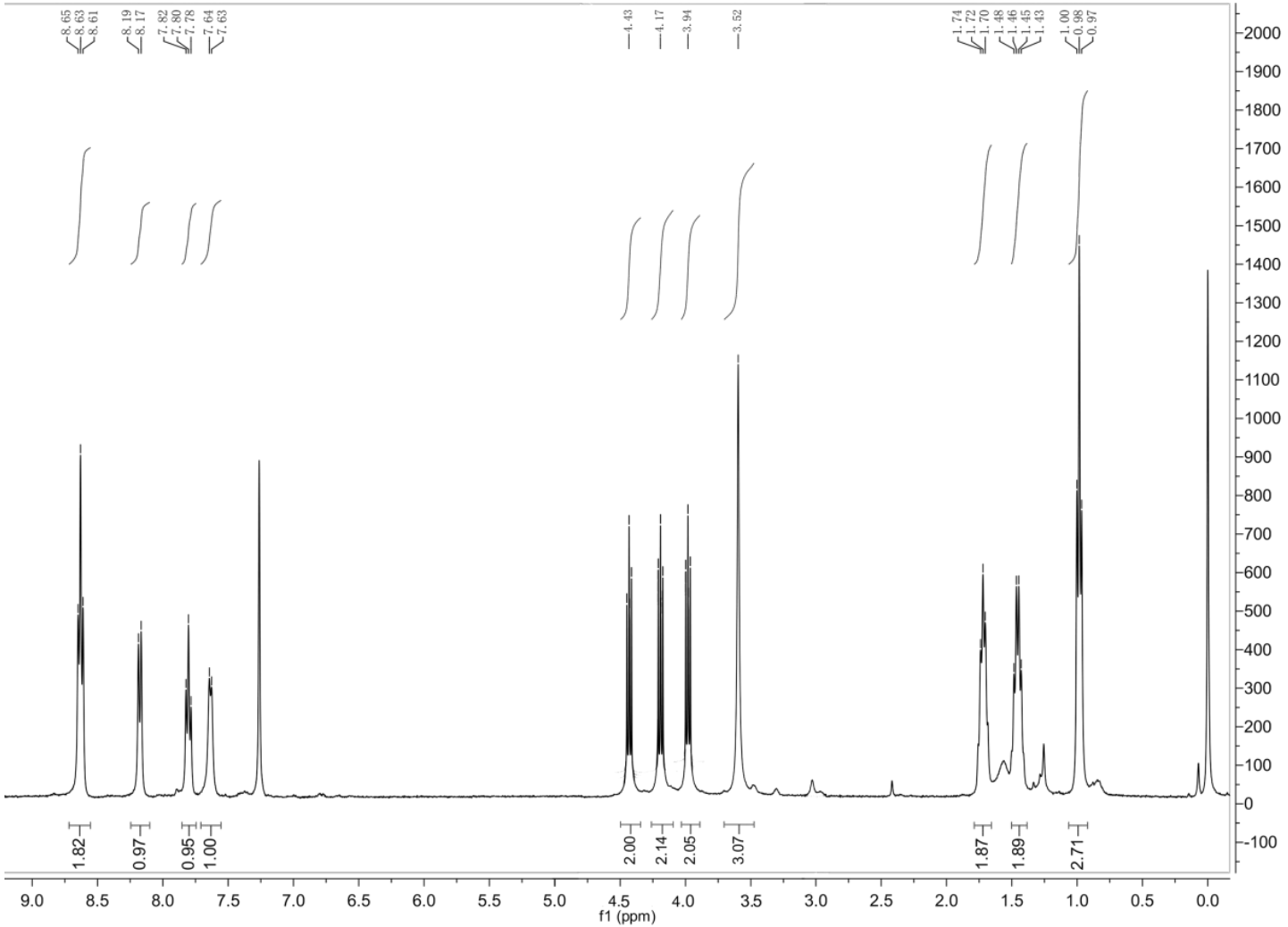

Figure S10. NIC-4 ^{1}H NMR

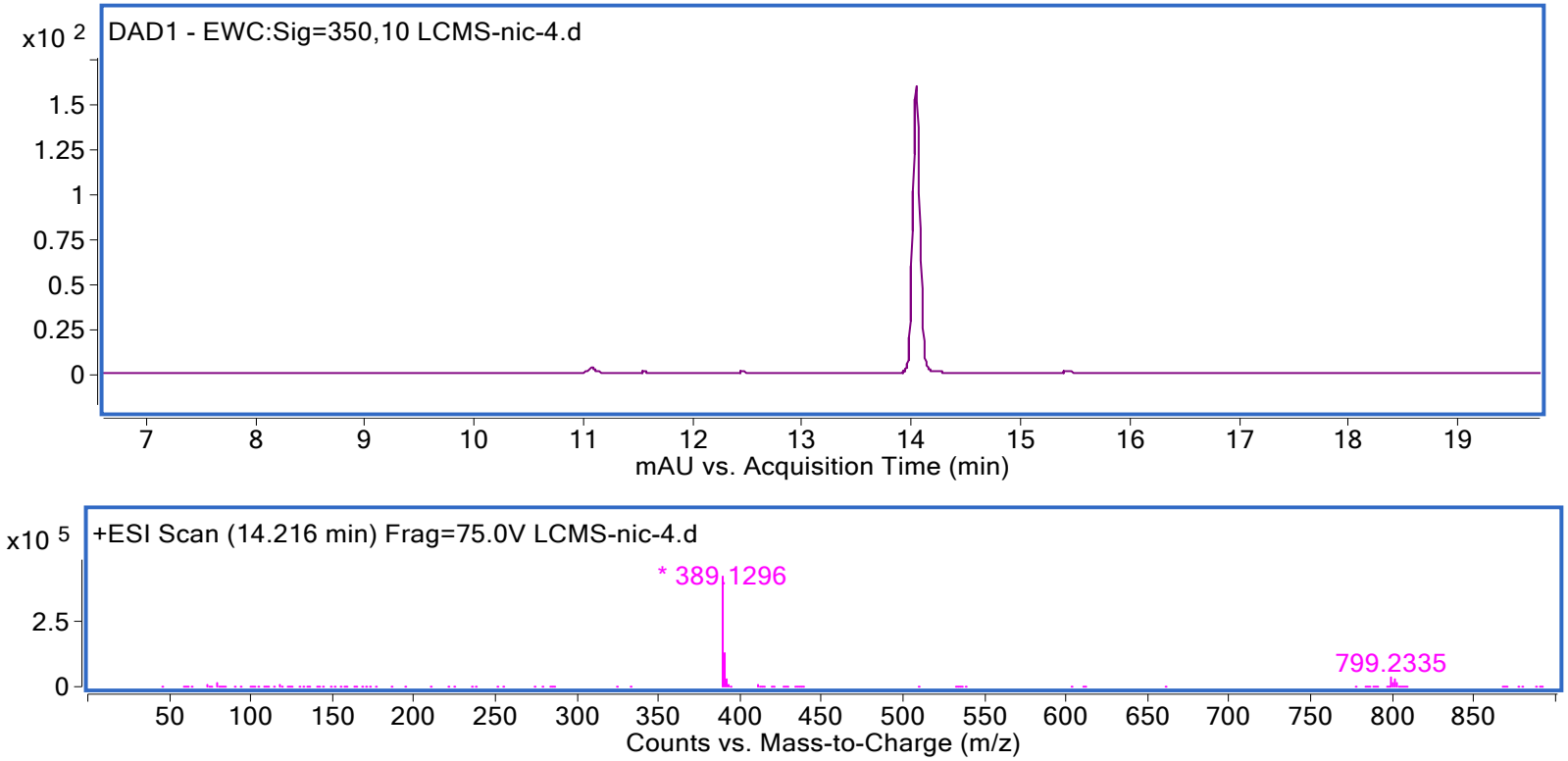

Figure S11. HPLC and HRMS of NIC-4

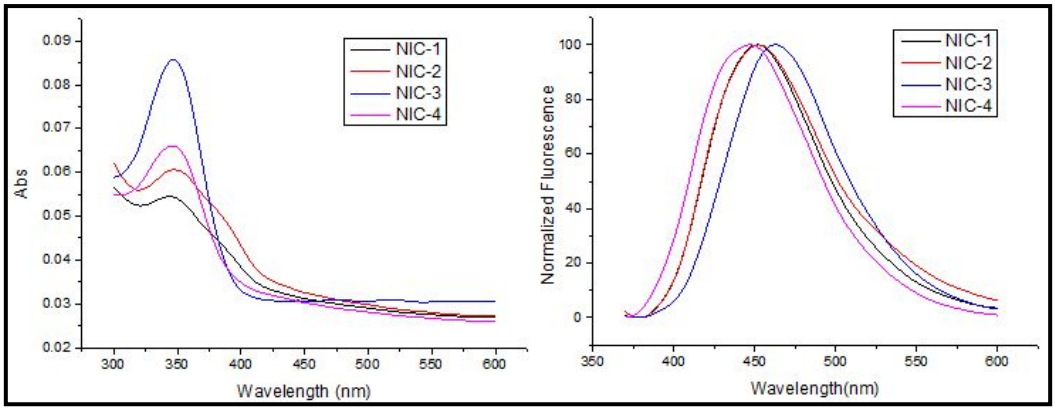

Figure S12. Spectral Properties of NIC1-4. Absorbance spectra of NIC1-4(left). Emission Spectra of NIC1-4(right).

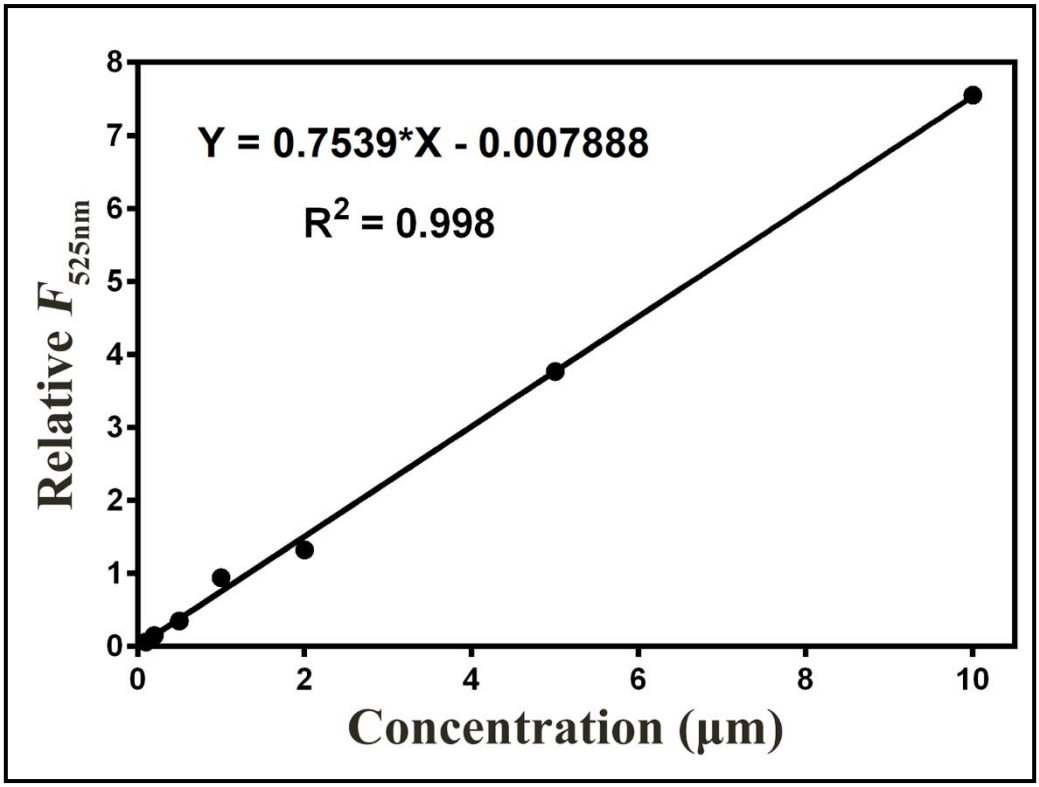

Figure S13. Correlation of product concentration of NIC series catalyzed by hCEs with relative fluorescence intensity

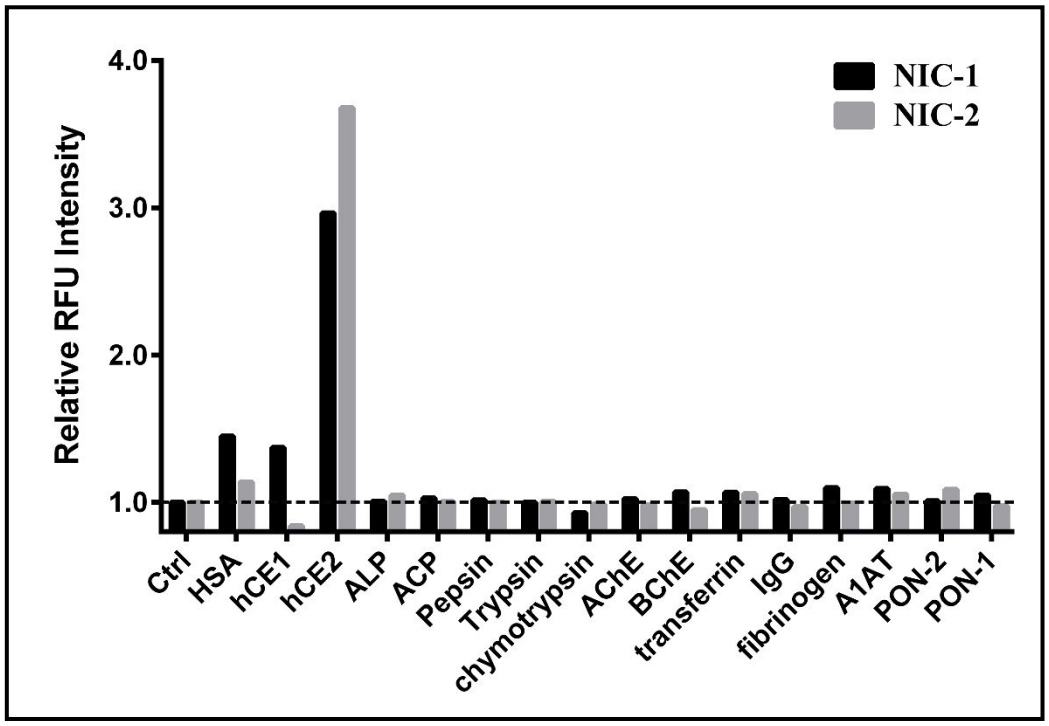

Figure S14. Targeting specificity of NIC1/2 upon different human esterases and plasma proteins (HSA at 2.5mg/mL, others at 100μg/mL)

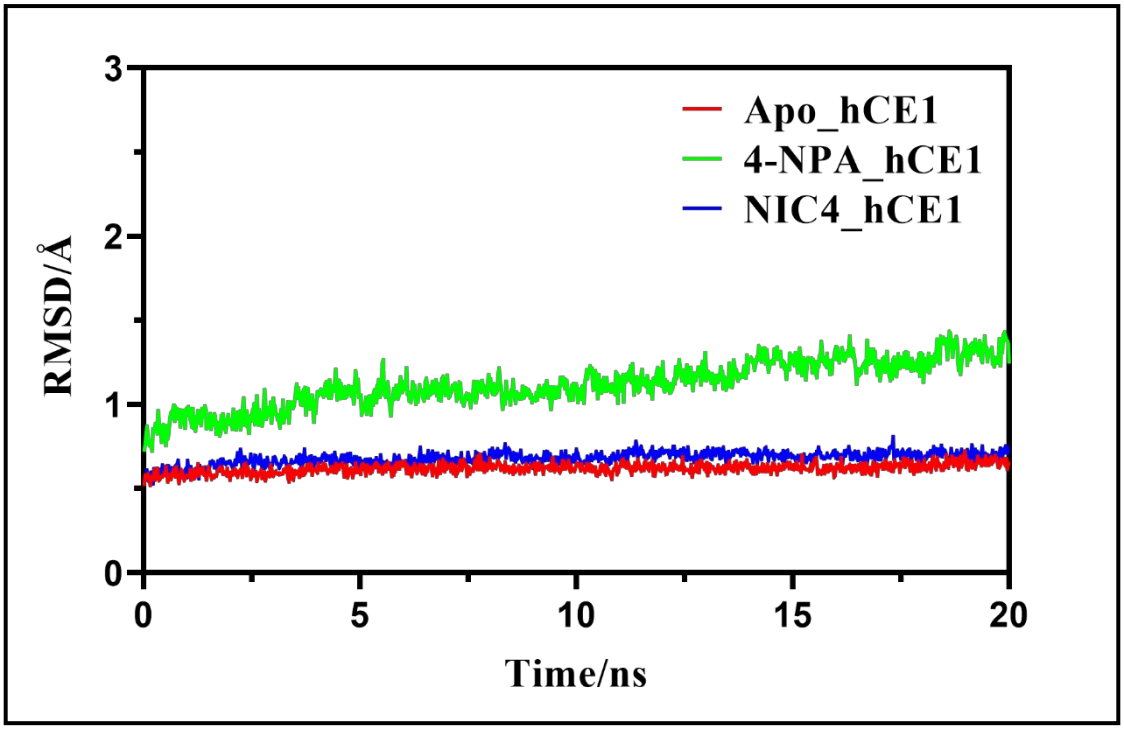

Figure S15. System RMSDs of 4-NPA_hCE1, NIC-4_hCE1 in comparison with Apo_hCE1 from 20ns MD simulations

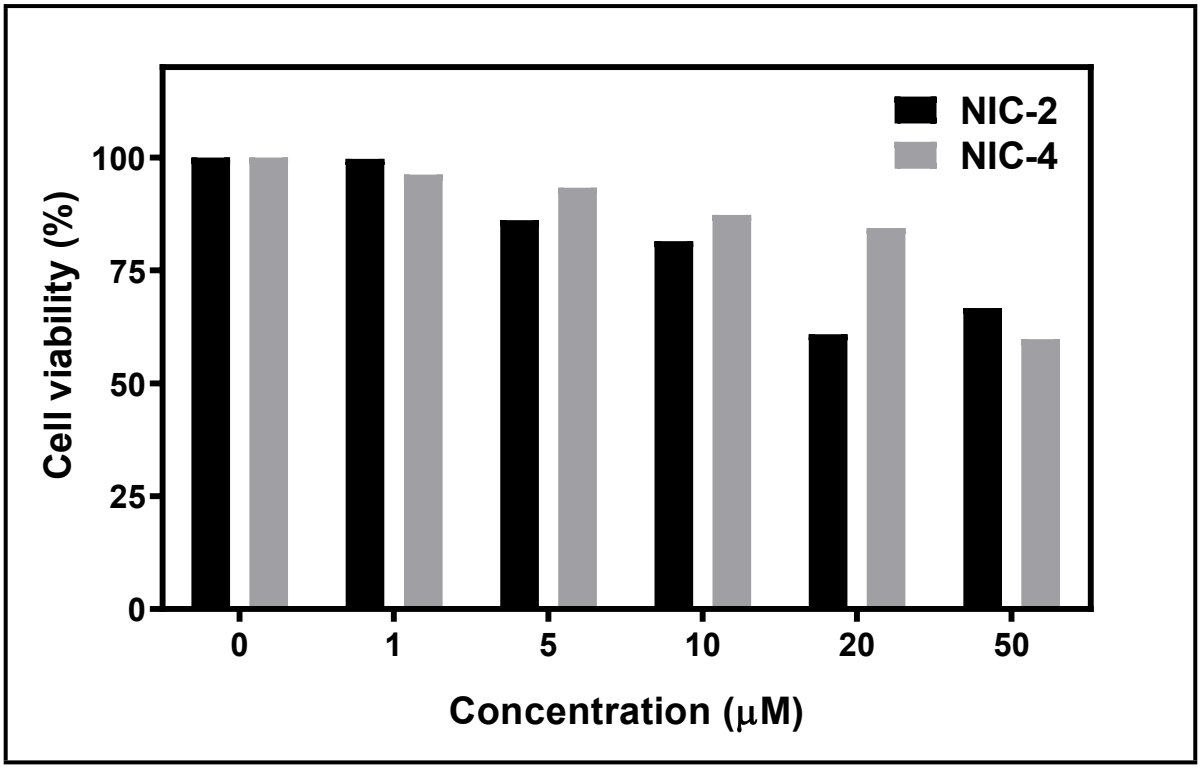

Figure S16. Cell viability of NIC-2/4 in HL 7402 cells

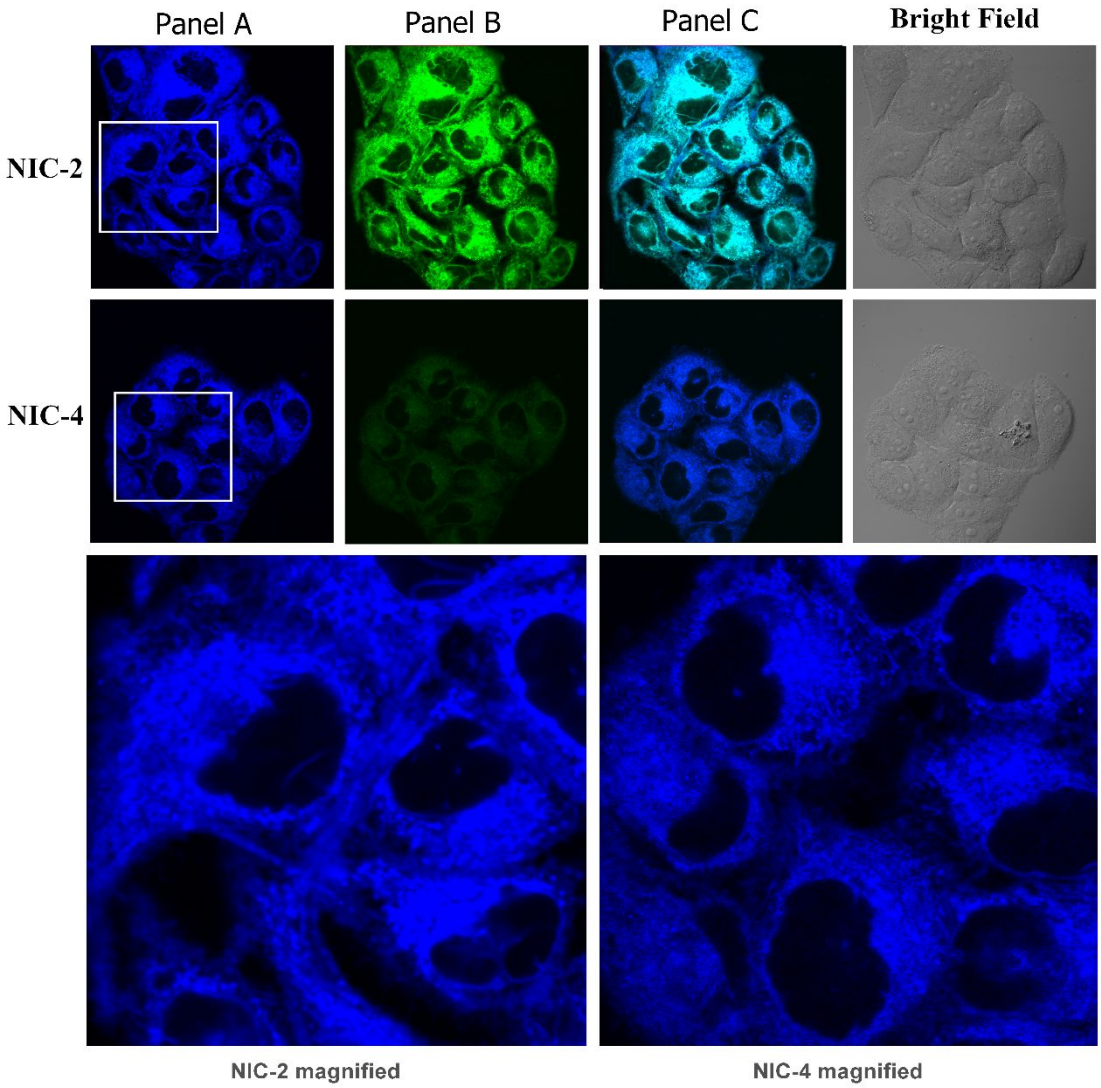

Figure S17. Imaging analysis for NIC-4/2 in living cell HL-7402. Representative images Panel A (the blue channel, excited with 405nm, collected with a 425−475 nm window.), Panel B (the green channel, excited with 405nm, collected with a 500-600 nm window), Panel C (merged channel of A/B, Regions of colocalization appear cyan in merged image). NIC-2 went through hydrolysis reflected by the fluorescence turn-on in the green channel, while NIC-4 remained unchanged in the green channel. Panel D (Bright field).

Table S2. Co-localization parameters of NIC-2/4 with commercially available antibody probe

	NIC-2	**NIC-4**
R_r [a]	0.378	0.749
R [b]	0.484	0.798
k_1 [c]	0.453	0.852
k_2 [d]	0.517	0.747
m_1 [e]	0.869	0.997
m_2 [f]	0.864	0.818

[a] Pearson's correlation

[b] Overlap coefficient parameter 1

[c] Overlap coefficient parameter 2

[d] Overlap coefficient parameter 3

[e] Co-localization (ch2 > 0)

[f] Co-localization (ch1 > 0)

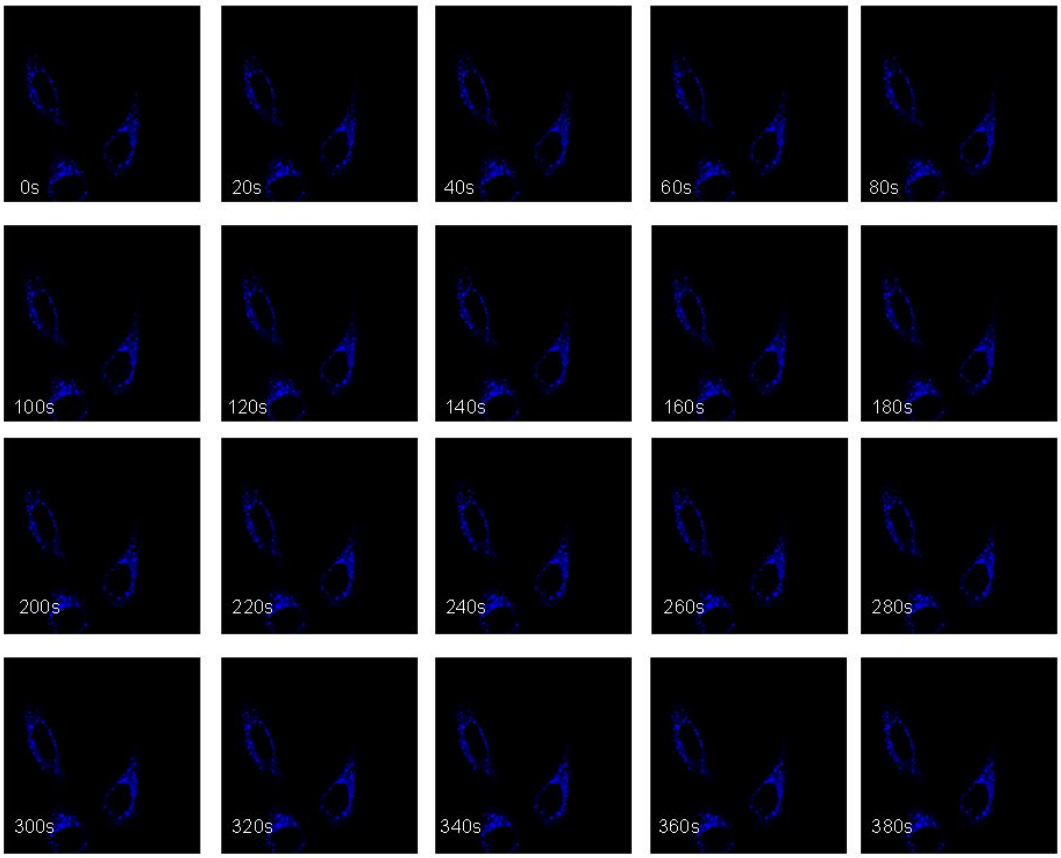

Figure S18. Time-lapse SIM images of hCE1 movement in living cells.

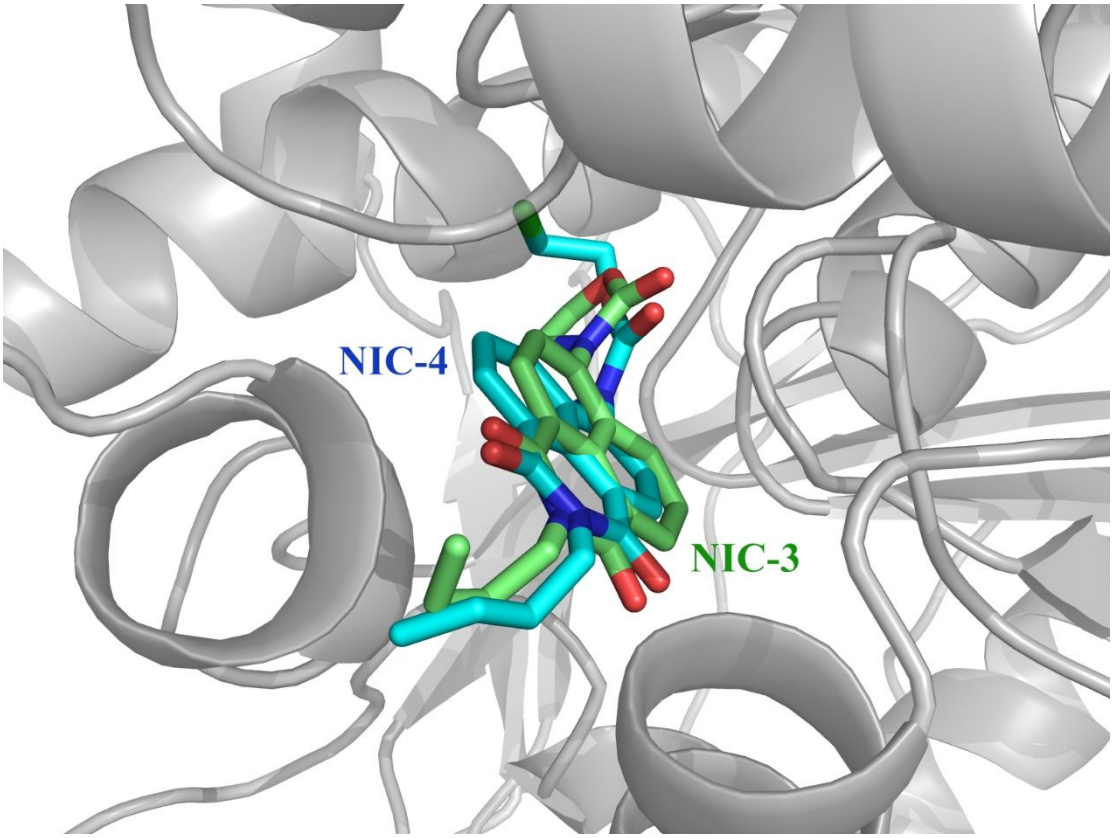

Figure S19. The docking result of NIC-3 and NIC-4 in the active pocket of hCE-2.

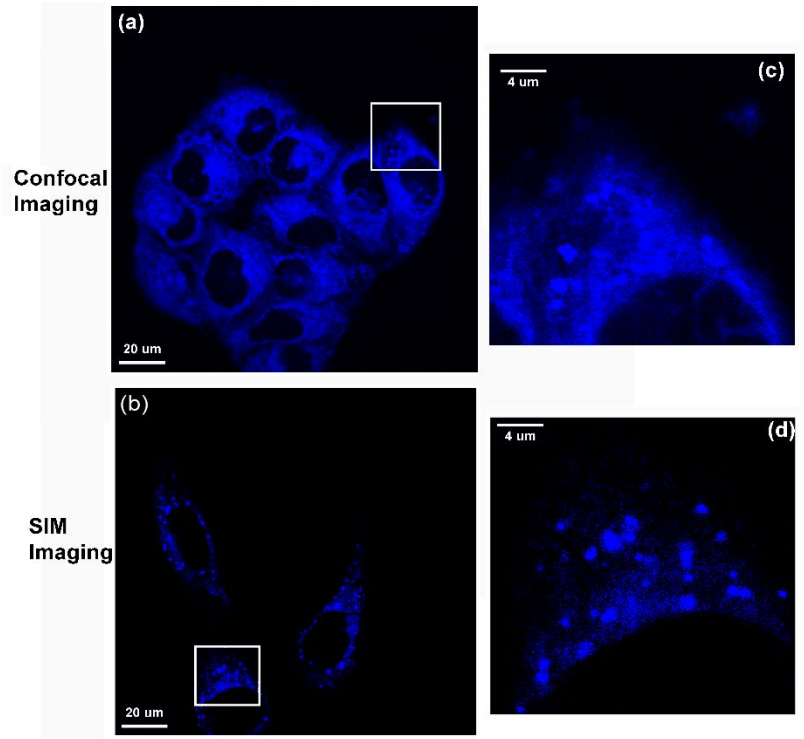

Figure S20. The resolution contrast of confocal imaging and SIM imaging. Confocal images of living cells (error bar=20 um) and the magnified view (error bar=4 um). SIM images of living cells (error bar=20 um) and the magnified view (error bar=4 um).

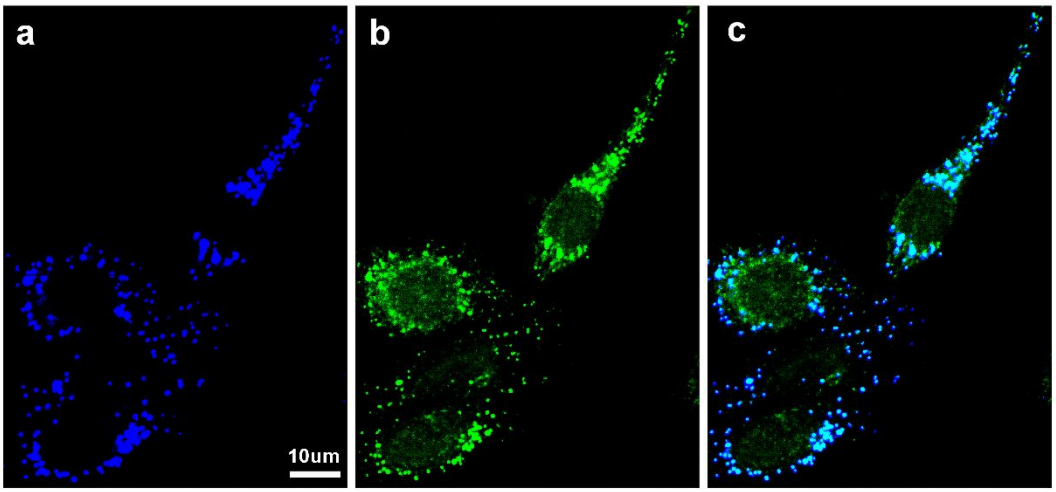

Figure S21. a) The SIM imaging results for NIC-4 ($\lambda_{ex} = 405$ nm, images collected from 425-475 nm blue channel) co-stained with commercially available antibody fluorescent probe targeting specifically hCE1 ($\lambda_{ex} = 488$ nm, images collected from 500-600 nm green channel). Regions of co-localization appeared in cyan (c).

Reference

1. C. D. Fleming, S. Bencharit, C. C. Edwards, J. L. Hyatt, L. Tsurkan, F. Bai, C. Fraga, C. L. Morton, E. L. Howard-Williams, P. M. Potter, M. R. Redinbo, Structural insights into drug processing by human carboxylesterase 1: Tamoxifen, mevastatin, and inhibition by benzil. *J Mol Biol* **352**, 165-177 (2005).
2. T. J. Dolinsky, J. E. Nielsen, J. A. McCammon, N. A. Baker, PDB2PQR: an automated pipeline for the setup of Poisson-Boltzmann electrostatics calculations. *Nucleic Acids Res* **32**, W665-W667 (2004).
3. J. A. Maier, C. Martinez, K. Kasavajhala, L. Wickstrom, K. E. Hauser, C. Simmerling, ff14SB: Improving the Accuracy of Protein Side Chain and Backbone Parameters from ff99SB. *J Chem Theory Comput* **11**, 3696-3713 (2015).
4. D. S. C. D.A. Case, I. T.E. Cheatham, T.A. Darden, R.E. Duke, T.J. Giese, H. Gohlke, A.W. Goetz, D. Greene, N. Homeyer, S. Izadi, A. Kovalenko, T.S. Lee, S. LeGrand, P. Li, C. Lin, J. Liu, T. Luchko, R. Luo, D. Mermelstein, K.M. Merz, G. Monard, H. Nguyen, I. Omelyan, A. Onufriev, F. Pan, R. Qi, D.R. Roe, A. Roitberg, C. Sagui, C.L. Simmerling, W.M. Botello-Smith, J. Swails, R.C. Walker, J. Wang, R.M. Wolf, X. Wu, L. Xiao, D.M. York and P. A. Kollman;, AMBER 16. (2017).
5. C. T. Lee, W. T. Yang, R. G. Parr, Development of the Colle-Salvetti Correlation-Energy Formula into a Functional of the Electron-Density. *Phys Rev B* **37**, 785-789 (1988).
6. A. D. Becke, Density-Functional Thermochemistry .1. The Effect of the Exchange-Only Gradient Correction. *J Chem Phys* **96**, 2155-2160 (1992).
7. A. D. Becke, Density-Functional Thermochemistry .3. The Role of Exact Exchange. *J Chem Phys* **98**, 5648-5652 (1993).
8. R. Ditchfield, W. J. Hehre, J. A. Pople, Self-Consistent Molecular-Orbital Methods .9. Extended Gaussian-Type Basis for Molecular-Orbital Studies of Organic Molecules. *J Chem Phys* **54**, 724-+ (1971).
9. G. W. T. M. J. Frisch, H. B. Schlegel, G. E. Scuseria, M. A. Robb, J. R. Cheeseman, G. Scalmani, V. Barone, G. A. Petersson, H. Nakatsuji, X. Li, M. Caricato, A. V. Marenich, J. Bloino, B. G. Janesko, R. Gomperts, B. Mennucci, H. P. Hratchian, J. V. Ortiz, A. F. Izmaylov, J. L. Sonnenberg, D. Williams-Young, F. Ding, F. Lipparini, F. Egidi, J. Goings, B. Peng, A. Petrone, T. Henderson, D. Ranasinghe, V. G. Zakrzewski, J. Gao, N. Rega, G. Zheng, W. Liang, M. Hada, M. Ehara, K. Toyota, R. Fukuda, J. Hasegawa, M. Ishida, T. Nakajima, Y. Honda, O. Kitao, H. Nakai, T. Vreven, K. Throssell, J. A. Montgomery, Jr., J. E. Peralta, F. Ogliaro, M. J. Bearpark, J. J. Heyd, E. N. Brothers, K. N. Kudin, V. N. Staroverov, T. A. Keith, R. Kobayashi, J. Normand, K. Raghavachari, A. P. Rendell, J. C. Burant, S. S. Iyengar, J. Tomasi, M. Cossi, J. M. Millam, M. Klene, C. Adamo, R. Cammi, J. W. Ochterski, R. L. Martin, K. Morokuma, O. Farkas, J. B. Foresman, and D. J. Fox, Gaussian, Inc., Wallingford CT., Gaussian 16, Revision A 03. (2016).
10. O. Trott, A. J. Olson, Software News and Update AutoDock Vina: Improving the Speed and Accuracy of Docking with a New Scoring Function, Efficient Optimization, and Multithreading. *J Comput Chem* **31**, 455-461 (2010).
11. W. L. Jorgensen, J. Chandrasekhar, J. D. Madura, R. W. Impey, M. L. Klein, Comparison of Simple Potential Functions for Simulating Liquid Water. *J Chem Phys* **79**, 926-935 (1983).
12. M. Gaus, A. Goez, M. Elstner, Parametrization and Benchmark of DFTB3 for Organic Molecules. *J Chem Theory Comput* **9**, 338-354 (2013).
13. U. Essmann, L. Perera, M. L. Berkowitz, T. Darden, H. Lee, L. G. Pedersen, A Smooth Particle Mesh Ewald Method. *J Chem Phys* **103**, 8577-8593 (1995).
14. J. P. Ryckaert, G. Ciccotti, H. J. C. Berendsen, Numerical-Integration of Cartesian Equations of Motion of a System with Constraints - Molecular-Dynamics of N-Alkanes. *J Comput Phys* **23**, 327-341 (1977).
15. K. I. Umehara, M. Zollinger, E. Kigondu, M. Witschi, C. Juif, F. Huth, H. Schiller, K. Chibale, G. Camenisch, Esterase phenotyping in human liver in vitro: specificity of carboxylesterase inhibitors. *Xenobiotica* **46**, 862-867 (2016).
16. S. K. Quinney, S. P. Sanghani, W. I. Davis, T. D. Hurley, Z. Sun, D. J. Murry, W. F. Bosron, Hydrolysis of capecitabine to 5 '-deoxy-5-fluorocytidine by human carboxylesterases and inhibition by loperamide. *J Pharmacol Exp Ther* **313**, 1011-1016 (2005).
17. L. W. Zou, Q. Jin, D. D. Wang, Q. K. Qian, D. C. Hao, G. B. Ge, L. Yang, Carboxylesterase

Inhibitors: An Update. *Curr Med Chem* **25**, 1627-1649 (2018).